PCCP

PAPER

View Article Online
View Journal | View Issue

Check for updates

Cite this: *Phys. Chem. Chem. Phys.*, 2017, **19**, 24284

Wheel-like, elongated, circular, and linear geometries in boron-based C_nB_{7-n} (n = 0–7) clusters: structural transitions and aromaticity†

Lin-Yan Feng and Hua-Jin Zhai*

Received 28th June 2017,
Accepted 15th August 2017

DOI: 10.1039/c7cp04327a

rsc.li/pccp

We report a quantum chemical study on the structural and bonding properties of a series of boron–carbon mixed clusters with seven atoms: C_nB_{7-n} (n = 0–7). Global-minimum structures were searched using the Coalescence Kick (CK) method, followed by B3LYP/6-311+G(d) calculations for full optimizations and energetics. Top candidate structures were further benchmarked at the single-point CCSD(T) level. Structural transitions were revealed to occur successively between wheel-like, elongated, circular, and linear geometries upon the increase of C contents in the clusters. Chemical bonding was elucidated *via* canonical molecular orbital (CMO) analyses and adaptive natural density partitioning (AdNDP). The number of delocalized electrons (σ plus π) in the clusters was shown to vary by one at a time from 5σ to 7σ, as well as from 3π to 6π, which allows aromaticity, antiaromaticity, and conflicting aromaticity to be precisely tuned according to the ($4n$ + 2) and $4n$ Hückel rules. Delocalized π and σ bonds and their electron counting appear to dictate the cluster structures of the whole series. Aromaticity in the systems was independently confirmed using nucleus-independent chemical shifts (NICSs). The monocyclic B_2C_5 cluster was shown to possess the greatest NICS values, consistent with its 6π plus 6σ electron countings for double aromaticity. Our analyses also shed light on the reason why C in the filled-hexagonal B_6C cluster occupies a peripheral site rather than the center and why C avoids hypercoordination in B–C binary clusters. A similar argument should be valid for other B–C clusters in prior reports, such as B_6C^{2-}, B_7C^-, and B_8C.

Published on 16 August 2017. Downloaded by Shanxi University on 10/31/2018 8:37:25 AM.

1. Introduction

Nanoclusters offer a fertile ground for diverse and exotic molecular structures as well as structural transitions, where every atom counts and every electron counts. Exploration of such cluster structures and rationalization of the structural changes are among key issues in physical chemistry and computational chemistry. In recent years, elemental boron clusters have been shown to adopt unique planar or quasi-planar geometries in a wide range of sizes up to 40 atoms,[1–16] which are unprecedented for any other element. The flat world of boron is associated with its intrinsic electron-deficiency, giving rise to (π and σ) aromaticity and antiaromaticity in boron clusters.[17] Among other developments in boron chemistry are boronyl clusters,[18–20] dynamic fluxionality (molecular Wankel motors[21,22] and tank treads[23,24]), borospherenes,[14–16,25] and borophenes.[26,27] Doping or mixing with other elements provides a new degree of freedom to tailor the structural, electronic, and bonding properties of boron clusters. To this end, element C is an ideal choice. Boron and carbon are nearest neighbors in the periodic table, and both elements form highly covalent chemical bonds. Also note that C is the prototypical element for aromaticity, in particular π aromaticity.

Thus, B–C mixed clusters are of interest in the exploration of new cluster structures. While boron clusters are planar or quasi-planar,[1–17] carbon clusters can have linear chain, cyclic ring, bowl, and fullerene cage structures. What if these two elements are mixed together? With regard to bonding, what would happen if the (π and σ) aromaticity and antiaromaticity of boron meet the π aromaticity of carbon? In B–C clusters, substitution of a B atom with C allows precise control of the number of valence electrons, one at a time, which can tune aromaticity and antiaromaticity in the system. So, how does π and σ aromaticity collectively govern the geometries of B–C clusters? What is the structural consequence of antiaromaticity, conflicting aromaticity, and double aromaticity? What are the possible structural transitions and what drives such transitions?

Nanocluster Laboratory, Institute of Molecular Science, Shanxi University, Taiyuan 030006, China. E-mail: hj.zhai@sxu.edu.cn

† Electronic supplementary information (ESI) available: Alternative optimized structures of C_nB_{7-n} (n = 1–6) clusters (Fig. S1–S6); NBO atomic charges for selected C_nB_{7-n} clusters and their anions (Fig. S7); canonical molecular orbitals (CMOs) of delocalized π and σ frameworks in C_nB_{7-n} (n = 0–6) (Fig. S8–S10); CMOs of the linear C_7 cluster (Fig. S11); and the complementary Clar-type adaptive natural density partitioning (AdNDP) scheme for B_3C_4, as well as the Kekule-type scheme for B_2C_5 and BC_6 (Fig. S12). See DOI: 10.1039/c7cp04327a

This journal is © the Owner Societies 2017

Published on 16 August 2017. Downloaded by Shanxi University on 10/31/2018 8:37:25 AM.

A number of experimental and theoretical studies on B–C mixed clusters are available in the recent literature. In 1995, using laser vaporization of a sample of graphite doped with $Na_2B_7O_4$, Wang *et al.*[28] generated BC_n^- anion clusters, as well as C_n^- and C_nBO^-, and they revealed a parity effect of BC_n^-, in which even n species are more stable. Presilla-Márquez *et al.*[29] observed linear BC_3 and B_2C_2 clusters and probed their structures by Fourier transform infrared spectroscopy and *ab initio* calculations. A recent joint photoelectron spectroscopy (PES) and computational study on $C_nB_{5-n}^-$ (n = 1–5) clusters[30] indicated that a planar-to-linear structural transition occurs between n = 2 and 3. For computational works, Chuchev *et al.*[31] studied BC_n and B_2C_n (n = 4–10) clusters at the B3LYP/6-311+G(d) level, in which they claimed that the global minimum (GM) is linear for n = 4, linear and cyclic geometries are almost isoenergetic for n = 5, and cyclic structures are stable for $n \geq 6$. Wang *et al.*[32] calculated B_nC (n = 1–7) clusters at the B3LYP level, suggesting that the C atom prefers to be at an apex site of the B structures and does not change the shapes of B clusters. Shao *et al.*[33] computed B_3C_n (n = 1–8) at the B3LYP level, suggesting that cyclic structures are favorable over linear and branching ones, as well as rings with exocyclic chains. It was also found that the species have (n + 1) π electrons with exception of B_3C_4 (6π electrons). The team also computed monocyclic B_4C_n (n = 2–9) clusters.[34] Wang *et al.*[35] studied planar B_5C_n (n = 1–7) clusters at the B3LYP level, suggesting that those with even n have higher stability. Pei *et al.*[36] probed planar multicoordinate carbon clusters, C_mB_n (m = 1–4; n = 4–8), *via* Basin-Hopping (BH) searches. Boldyrev and coworkers reported structural changes in $C_nB_{8-n}^-$ (n = 1–8) and $C_nB_{10-n}^-$ (n = 3–10),[37,38] from molecular wheel to monocyclic ring to linear species. It is stressed that of all these theoretical works, ''unbiased'' computer searches for GM structures were done only in ref. 35–38. Additional computational works were performed on the structures, potential energy surfaces, and stability of BC_n (n = 3–5), $B_4C^{0/+}$, B_5C, B_2C_4, B_3C_3, and B_4C_2 clusters using different methods.[39–45]

In the current contribution, we report a quantum chemical study on a series of seven-atom boron–carbon mixed clusters: C_nB_{7-n} (n = 0–7). These clusters are intriguing for a couple of reasons. First, the bare B_7^- cluster[4] was experimentally shown to possess wheel-like and elongated conformations, with three isomers co-existing in the cluster beam in the gas phase, and in the $B_7Au_2^-$ alloy cluster,[46] the elongated conformation is selectively stabilized as the sole isomer. In contrast, the bare C_7 cluster has a distinctly different linear structure. Therefore, a series of structural transitions are anticipated with the increase of C component in C_nB_{7-n} (n = 0–7). Second, the shapes of B_7^- and B_7 isomers are known to depend sensitively on the nature of delocalized π and σ frameworks (as well as electronic states). In C_nB_{7-n} (n = 0–7) clusters, the delocalized π and σ electrons are tuned precisely, allowing us to address how the electron countings dictate cluster conformations. Third, there is a long-standing open question why C avoids hypercoordination in a number of specific B–C clusters, for which the present system can offer mechanistic insight. Herein, our explorations of the potential energy surfaces *via* global structural searches reveal wheel-like, elongated, circular, and linear geometries for the C_nB_{7-n} (n = 0–7) clusters. Chemical bonding analyses indicate that (π and σ) aromaticity, antiaromaticity, conflicting aromaticity, and double aromaticity are present from species to species, which govern the cluster conformations as well as structural transitions along the series.

2. Computational methods

The GM structures of C_nB_{7-n} (n = 1–6) neutral clusters were explored using an unbiased Coalescence Kick (CK) method;[47–49] those of B_7 and C_7 were taken from literature[4,60] and re-optimized for the sake of completeness. The CK searches were conducted for both singlet and triplet states for clusters with an odd number of C atoms, and a total of 3500 stationary points were probed for each cluster. For clusters with even number of C atoms, only doublet states were searched: 2000 stationary points for each species. Subsequently, candidate low-lying isomers were fully re-optimized at the B3LYP/6-311+G(d) level along with vibrational frequency calculations, using the Gaussian 09 package.[50]

To further evaluate the energetics, top lowest-lying isomers close in energy were benchmarked *via* single-point CCSD(T) calculations[51–54] at the B3LYP/6-311+G(d) geometries. Chemical bonding in the GM clusters was elucidated using natural bond orbital (NBO)[55] atomic charges, canonical molecular orbital (CMO) analyses, adaptive natural density partitioning (AdNDP),[56] and nucleus-independent chemical shifts (NICSs).[57] Since the AdNDP method is not sensitive to the basis set used, we chose the 6-31G basis set for AdNDP calculations. Molecular structures, CMOs, and AdNDP results were visualized using the Molekel 5.4 program.[58] Born–Oppenheimer molecular dynamics (BOMD) simulations were performed using the CP2K software package.[59]

3. Results

3.1. B_7 and B_6C

The GM structures of C_nB_{7-n} (n = 1–6) neutral clusters at the B3LYP level, as established in this work, are illustrated in Fig. 1 and 2, along with those of B_7 and C_7 taken from the literature[4,60] and re-optimized at the B3LYP level. Zhai *et al.*[4] studied the electronic structure and bonding of B_7 and B_7^- *via* anion PES and *ab initio* calculations, suggesting that two almost degenerate pyramidal (C_{6v}, $^3A_1$) and (C_{2v}, $^1A_1$) structures, as well as a planar, elongated (C_{2v}, $^1A_1$) isomer, co-exist in the experimental B_7^- cluster beam. For the neutral cluster, the GM is clearly the open-shell, pyramidal B_7 (C_{2v}, $^2B_2$), whose re-optimized geometry is shown in Fig. 1(a). The B_7 cluster is quasi-planar and wheel-like, featuring a hexacoordinate B center, which is encircled by a hexagonal ring. It serves as the natural starting point for structural evolution of the C_nB_{7-n} (n = 0–7) series.

The B_6C cluster assumes a C_s ($^1A'$) GM (Fig. 1(b)), which can be straightforwardly constructed from B_7 (C_{2v}, $^2B_2$) *via* substitution of one peripheral B site with C, leading to a lower C_s symmetry. The B2B3 link in B_6C shrinks slightly by 0.02 Å relative to that in B_7. In contrast, the B1B2 link expands by 0.02 Å. The overall

Published on 16 August 2017. Downloaded by Shanxi University on 10/31/2018 8:37:25 AM.

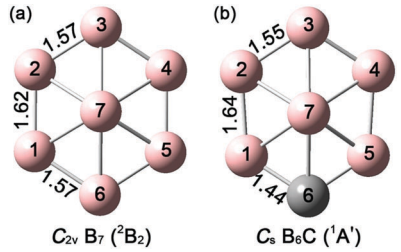

Fig. 1 Optimized global-minimum (GM) structures at the B3LYP/6-311+G(d) level for (a) B_7 (C_{2v}, $^2B_2$) and (b) B_6C (C_s, $^1A'$). Bond distances are given in Å. The B atoms are marked in pink and C in gray.

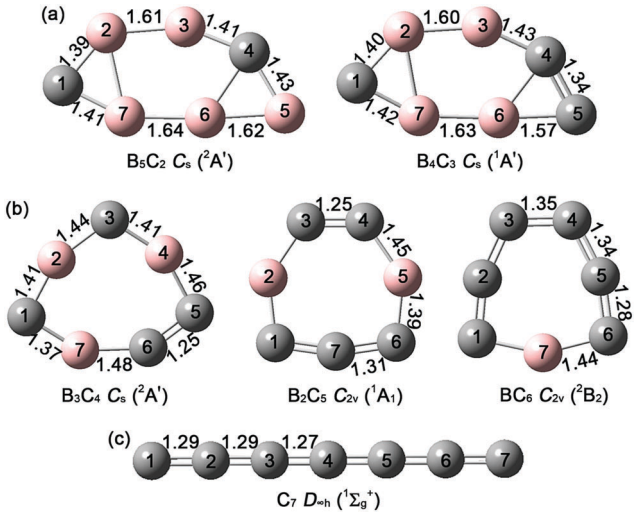

Fig. 2 Optimized GM structures at the B3LYP/6-311+G(d) level for (a) B_5C_2 (C_s, $^2A'$) and B_4C_3 (C_s, $^1A'$), (b) B_3C_4 (C_s, $^2A'$), B_2C_5 (C_{2v}, $^1A_1$), and BC_6 (C_{2v}, $^2B_2$), and (c) C_7 ($D_{\infty h}$, $^1\Sigma_g^+$). Bond distances are given in Å. The B atoms are marked in pink and C in gray.

out-of-plane distortion also deteriorates slightly: 0.64 Å for B_7 *versus* 0.69 Å for B_6C. We note that quasi-planarity is routine in boron clusters,[1–17] which is due to the fact that peripheral B atoms are bound, in addition to delocalized π and σ frameworks, by localized two-center two-electron (2c–2e) σ bonds; whereas the radial B–B links are held together by delocalized bonding only. Consequently, the radial B–B distances are much longer than the peripheral ones. In other words, a fastened peripheral B_6 ring is not large enough to accommodate a B center in a perfectly planar fashion. For the doped B_6C cluster (Fig. 1(b)), the bond distances of B–C links (both peripheral and radial) differ significantly from those of B–B links, furthering the structural distortions from high symmetry. The above qualitative arguments should as well be valid for other low-symmetry clusters in this study. Alternatively, such non-planar distortions may be understood using the pseudo Jahn–Teller theory proposed by Datta and coworkers, which takes into consideration the strong vibrational coupling between occupied molecular orbitals (OMOs) and unoccupied molecular orbitals (UMOs).[61–66] This topic should be of interest for pursuit in full detail, which is beyond the scope of the current study. Note that the B_6C (C_s, $^1A'$) GM is in line with a prior study by Pei *et al.*,[36] who probed planar multicoordinate carbon and identified the lowest-energy isomers of C_mB_n clusters (m = 1–4; n = 4–8) *via* BH searches, including B_6C. However, our results disagree with those of Wang *et al.*[32] who concluded that elongated isomer **a2** (Fig. S1, ESI†) is the lowest-energy structure. Apparently, no computer searches were performed in ref. 32.

Selected alternative structures of B_6C are shown in Fig. S1 (ESI†), where the second to fourth isomers all adopt elongated structures. The nearest competitive one, **a2** (C_s, $^1A'$), is 4.74 kcal mol^{-1} above the GM at the single-point CCSD(T) level. A triplet **a5** (C_s, $^3A''$) state is relevant to the GM, yet it is 17.46 kcal mol^{-1} higher in energy. Among the higher isomers is wheel-like **a16** (C_{2v}, $^1A_1$), which differs from the GM in the position of C only. Remarkably, moving the C atom from the peripheral ring to the hexacoordinate center elevates the energetics of B_6C by as much as 34.62 kcal mol^{-1} at the B3LYP level, although **a16** seems to be ideal and elegant structure-wise.

According to the latest recommended covalent radii,[67] the upper bound of bond distances for single B–B, double B=B, and triple B≡B bonds is 1.70, 1.56, and 1.46 Å, respectively. Thus, the peripheral BB distances of 1.55 and 1.57 Å in Fig. 1 are close to double bonds, whereas those of 1.62 and 1.64 Å fall in the regime of single bonds (albeit with certain double bond character). Likewise, the peripheral B–C bonds (1.44 Å) are close to the upper bound of the B=C double bond (1.45 Å).[67] The above analyses suggest that, along with classical 2c–2e B–B or B–C single bonds, there exist delocalized π and/or σ frameworks in these clusters.

3.2. B_5C_2 and B_4C_3

As shown in Fig. 2(a), the GM structures of B_5C_2 and B_4C_3 adopt elongated geometries of C_s ($^2A'$) and C_s ($^1A'$), respectively. These structures may be traced back to the second isomer of B_6C, that is, **a2** (C_s, $^1A'$; Fig. S1, ESI†). Upon substitution of a second B in B_6C **a2** with C, or a B_2 dimer with C_2, one readily generates the GM structures of B_5C_2 and B_4C_3. Likewise, B_5C_2 and B_4C_3 can be related to the elongated isomer of B_7^-.[4] Note that the C_s ($^2A'$) GM of B_5C_2 is consistent with that of Wang and coworkers,[35] who studied the B_5C_n (n = 1–7) series. Shao *et al.*[34] computed monocyclic B_4C_n (n = 2–9) clusters at the B3LYP/6-311+G(d) level, albeit without computer searches, and concluded that the most stable monocyclic structure of B_4C_3 is **c2** (C_{2v}, $^3B_1$) (Fig. S3, ESI†). Our B3LYP and CCSD(T) data consistently show that **c2** is not the GM.

The C component in the GM structures of B_5C_2 and B_4C_3 is divided into isolated C atoms and the C_2 dimer, which are separated from each other. The B–B bonds have distances of 1.60–1.64 Å, which correspond to the longer ones in the peripheral rings of B_7 and B_6C (Fig. 1). Thus, delocalized π and σ bonding appears to contribute very little to B–B bonds in B_5C_2 and B_4C_3. In contrast, B–C bonds fall into two categories: shorter ones (1.39–1.43 Å) *versus* a longer one (1.57 Å). The former are close to B=C double bonds, whereas the latter is essentially a B–C single bond. The C–C bond in B_4C_3 is 1.34 Å, close to the upper bound of a C=C double bond (1.34 Å).[67]

 This journal is © the Owner Societies 2017

Published on 16 August 2017. Downloaded by Shanxi University on 10/31/2018 8:37:25 AM.

Alternative low-lying structures of B_5C_2 and B_4C_3 are collected in Fig. S2 and S3 (ESI†). The potential energy surface of B_5C_2 is dominated by isomers with a seven-membered ring in an elongated shape. Indeed, this is true for all top five structures, as well as for 13 out of top 20 structures (Fig. S2, ESI†). The lowest-energy structure with a hexacoordinate B center is **b6** (C_s, $^2A''$), being 18.88 kcal mol^{-1} above the GM at the B3LYP level. For the B_4C_3 cluster, low-lying structures are also dominated by isomers with a seven-membered ring, which possess either an elongated (12 out of top 20 isomers) or a circular (6 out of top 20 isomers) conformation. Wheel-like structure **c5** (C_{3v}, $^1A_1$) ranks number 5, being 14.62 kcal mol^{-1} above the GM. Note that in wheel-like **b6** and **c5**, the C atoms are all located on the peripheral ring and the C atoms manage to be separated as far away as possible from each other.

3.3. B_3C_4, B_2C_5, and BC_6

The GM structures of B_3C_4, B_2C_5, and BC_6 clusters are monocyclic rings, as illustrated in Fig. 2(b). These are sort of circular in shape, in contrast to the elongated shape for B_5C_2 and B_4C_3. The B_3C_4 (C_s, $^2A'$) GM is in line with that identified by Shao and coworkers,[33] who explored the B_3C_n (n = 1–8) series albeit without systematic structural searches. In terms of bond distances, the B–C distances are in the regime of 1.37–1.48 Å, close to double bonds. The C–C distances lie in the regime of 1.25–1.35 Å, which are beyond single bonds. In particular, those of C_2 units (1.25 Å) appear to be even shorter than the C=C double bond. Alternative optimized structures of B_3C_4, B_2C_5, and BC_6 are shown in Fig. S4–S6 (ESI†), which favor monocyclic ring structures, followed by linear ones at higher energies. Interestingly, the energetics of the linear isomer becomes competitive with the increase of C component. The lowest-energy linear isomer is 47.78, 47.49, and 18.52 kcal mol^{-1} above the monocyclic GM structures, respectively. No structures are revealed with a multicoordinate central B/C atom for these species, in contrast to B_7 and B_6C (Fig. 1).

3.4. C_7

The C_7 cluster was previously studied both experimentally and theoretically.[60] Its well-known linear $D_{\infty h}$ ($^1\Sigma_g^+$) structure is re-optimized at the B3LYP level and illustrated in Fig. 2(c). The C–C distances are 1.27–1.29 Å, typical for double bonds.[67]

4. Discussion

4.1. Wheel-like, elongated, circular, and linear geometries in C_nB_{7-n} (n = 0–7) clusters

The C_nB_{7-n} (n = 0–7) series of B–C binary clusters have a rich variety of conformations with the increase of C component, starting from the bare B_7 cluster with a wheel-like shape and eventually reaching a one-dimensional C_7 linear chain. In between them, there exist three categories of B–C mixed clusters: (1) wheel-like B_6C featuring a hexacoordinate B center and a hexagonal ring, in which C occupies a peripheral site to avoid hypercoordination; (2) seven-membered ring B_5C_2 and B_4C_3 clusters with an elongated shape; (3) monocyclic, circular B_3C_4, B_2C_5, and BC_6 clusters. Three kinds of structural transitions occur along the C_nB_{7-n} (n = 0–7) series, making them remarkable examples to demonstrate the structural richness in boron-based clusters and how structures can be controlled or tuned in B–C binary clusters. Note that substitution of one B with C only increases the number of electrons by one. Thus, the present system allows the control of valence electrons with precision: one at a time.

Along the C_nB_{7-n} (n = 0–7) series, the C atoms have a clear tendency to be separated from each other, rather than clustering together as one C_n structural block, although C_n chains are predominating species for small, bare C clusters. For C_nB_{7-n} (n = 1–5), the C atoms are islanded as C, C_2, and C_3 groups and the islands tend to be as small as possible. The two C atoms in B_5C_2 are isolated from each other and positioned far apart, as are the C and C_2 groups in B_4C_3 (Fig. 2(a)). Most remarkably, four C atoms in B_3C_4 manage to fragment into three C, C, and C_2 groups, being isolated from each other by three B atoms. As the C component increases, slightly larger islands such as C_3 appear in B_2C_5. Only in the ring BC_6 cluster the C atoms form a single chain, because there are no alternative options.

The C_nB_{7-n} (n = 0–7) clusters are highly covalent bound species, and thus their stability at finite temperature is generally not an issue of concern. However, in response to the request from one reviewer, we have performed a BOMD simulation[59] at high temperature, using B_5C_2 as example. The BOMD simulation was performed at a temperature of 1000 K for 20 ps, at the PBE/DZVP level. The results confirm that the cluster is indeed robust even at such a high temperature, maintaining its overall shape and structural integrity during the simulation. Of course, the results are as anticipated and not surprising.

4.2. Natural atomic charges: electrostatics in B–C mixed clusters

Why are the C atoms in C_nB_{7-n} (n = 0–7) fragmented into small islands (Fig. 2)? Why are the C islands isolated from each other? Natural atomic charges from the NBO analyses offer some clue for the issue. Fig. 3 shows the NBO atomic charges for these species. While people may believe that the B–C mixed clusters are highly covalent bound systems, NBO charges indicate that such a notion is not exactly true. Indeed, the C islands (C, C_2, and C_3) all carry a substantial amount of negative charges, despite the fact that C_nB_{7-n} (n = 0–7) clusters are overall neutral in charge state. Specifically, an isolated C atom in C_nB_{7-n} has from −0.56 up to −0.89 $|e|$, a C_2 group collectively carries a charge of −0.49 to −0.65 $|e|$, and a C_3 group has a net charge of −0.85 $|e|$. Note that in a C_2 or C_3 group, the charge is not uniformly distributed among the C atoms; the middle C atom in C_3 can actually carry a slight positive charge (+0.15 $|e|$). Remarkably, even the C_7 linear chain exhibits a non-uniform charge distribution, with the C2/C4/C6 atoms being negatively charged by −0.11 or −0.43 $|e|$. In short, the C islands in C_nB_{7-n} (n = 0–7) normally carry negative charges.

As for B atoms, those interacting directly with C islands are positively charged. The magnitude of charge varies depending on the shape of the cluster, as well as the coordination environment

Published on 16 August 2017. Downloaded by Shanxi University on 10/31/2018 8:37:25 AM.

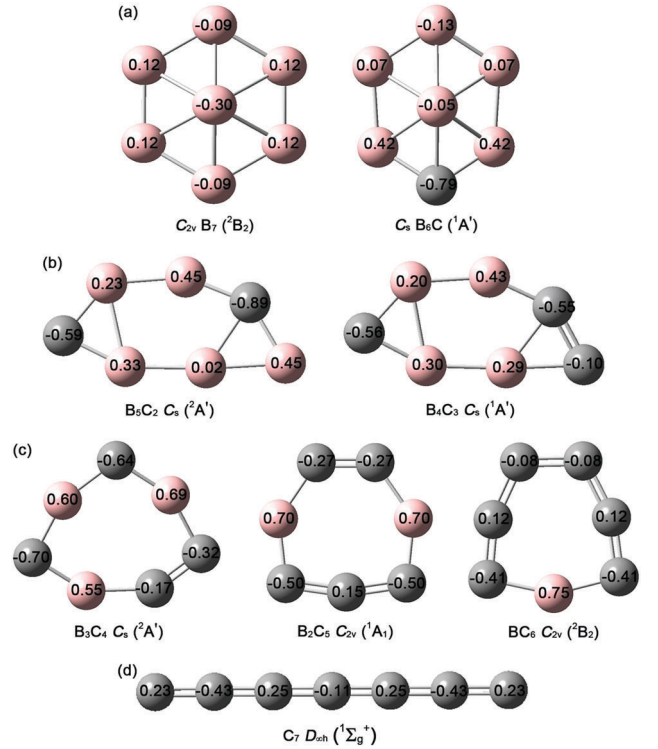

Fig. 3 NBO atomic charges (in $|e|$) for the GM structures of C_nB_{7-n} (n = 0–7) clusters.

of a B atom with the C islands. In wheel-like B_6C, two peripheral B atoms each share half of the charge (+0.42 $|e|$), collectively balancing the negative C site (−0.79 $|e|$). For elongated B_5C_2 and B_4C_3, the negative charge on each C or C_2 island is also balanced by two nearest B atoms, whose charges span a regime from +0.20 to +0.45 $|e|$. For circular B_3C_4, B_2C_5, and BC_6 clusters, the B atoms are isolated and each B atom carries a substantial positive charge of +0.55 to +0.75 $|e|$, countering the negative charges of two neighboring C islands. The above analyses show that remarkable intramolecular charge redistributions occur in the B–C mixed clusters and that the charge transfers are relatively local processes (presumably relevant to 2c–2e B–C σ bonds). The intramolecular charge transfers are attributed to the difference in electronegativity between B and C (2.04 *versus* 2.55; Pauling scale). Thus, from an electrostatic point-of-view, the C atoms in C_nB_{7-n} indeed should be divided into islands as small as possible and distributed as dispersedly as possible, which help manage intramolecular Coulomb repulsion that is present in the system. Furthermore, the disperse distribution of C atoms also facilitates the formation and optimization of delocalized π and σ frameworks, which make global uses of electrons from all B/C atoms. In contrast, a segregated B–C cluster would otherwise lead to electron-poor *versus* electron-rich regimes, which are not optimal, if not impossible, for globally delocalized bonding.

Interestingly but not surprisingly, the NBO atomic charges also offer intuitive hints where the next C should go in C_nB_{7-n} (n = 0–7); a few examples are presented in Fig. S7 (ESI†). As shown in Fig. S7(a) (ESI†), while the B atoms in the peripheral ring in B_7 cluster are practically neutral, the B6 and B3 sites in the B_7^- anion are markedly negatively charged (due to the extra electron). Since B_6C is isovalent to B_7^- and the C center is also highly electronegative, it is natural that C should go to B6 or B3 sites in B_7^-, leading to the B_6C (C_s, $^1A'$) GM (Fig. 1(b)). Likewise, the charge distributions in B_5C_2 and $B_5C_2^-$ (Fig. S7(b), ESI†) indicate that the extra charge in $B_5C_2^-$ contributes primarily to the B5 corner. As a consequence, the third C atom in B_4C_3 goes to the B5 site in B_5C_2, exactly generating the B_4C_3 (C_s, $^1A'$) GM. For B_3C_4 and $B_3C_4^-$, the B2 site in $B_3C_4^-$ carries the largest charge, and it is slightly more favorable for C to replace B2 (Fig. 2(b)), although other options appear to be competitive. This leads to the B_2C_5 (C_{2v}, $^1A_1$) GM.

4.3. Aromaticity, antiaromaticity, and conflicting aromaticity: π and σ

To fully rationalize the structural transitions in the C_nB_{7-n} (n = 0–7) clusters, it is essential to perform in-depth chemical bonding analyses. We chose to carry out CMO and AdNDP analyses, as well as NICS calculations, which collectively offer a concerted bonding picture for this series of clusters. The nature of bonding in the wheel-like B_7 cluster (Fig. 1) is well understood in prior work.[4] With 21 valence electrons, the occupied CMOs of B_7 include six for peripheral 2c–2e Lewis B–B σ bonds; the remaining five CMOs constitute the global bonding (σ and π). Specifically, the σ framework has three CMOs: HOMO−1, HOMO−2, and HOMO−4 (Fig. S8, ESI†). HOMO−4 is completely delocalized and bonding, whereas HOMO−1 and HOMO−2 are partially bonding/antibonding. This σ combination is in the spirit of the prototypical π sextet in benzene, endowing B_7 with σ aromaticity. Note that the 6σ electron counting conforms to the ($4n$ + 2) Hückel rule. The delocalized π framework involves two CMOs: HOMO and HOMO−5. HOMO−5 is again completely delocalized and bonding and the HOMO is partially bonding/antibonding, suggesting that B_7^+ can be a 2π aromatic system. For the B_7 neutral cluster, the 3π electron counting does not satisfy the Hückel rule exactly, leading to structural distortion to C_{2v} (Fig. 1(a)) due to the Jahn–Teller effect. In summary, B_7 has delocalized π and σ frameworks, whose 6σ electron counting renders σ aromaticity and 3π counting deviates from the Hückel rule.

The above bonding picture of B_7 is borne out by AdNDP analysis; see Fig. 4(a). AdNDP is an extension of the NBO analysis. It represents the electronic structure of a molecule in terms of n-center two-electron (nc–2e) bonds, with n ranging from one to the total number of atoms in the molecule. AdNDP analysis thus recovers not only the Lewis bonding elements (lone pairs and 2c–2e bonds), but also delocalized nc–2e bonds. Since the current version of the AdNDP program applies to closed-shell systems only, we use the B_7^- anion to represent B_7. Indeed, AdNDP recovers six 2c–2e B–B σ bonds, a delocalized σ sextet, and two delocalized 7c–2e π bonds, in line with the CMO analysis.

Moving along the C_nB_{7-n} (n = 1–7) series, the number of electrons increases by one at a time, and the species have from 22 up to 28 electrons. For two-dimensional structures, either

 This journal is © the Owner Societies 2017

Published on 16 August 2017. Downloaded by Shanxi University on 10/31/2018 8:37:25 AM.

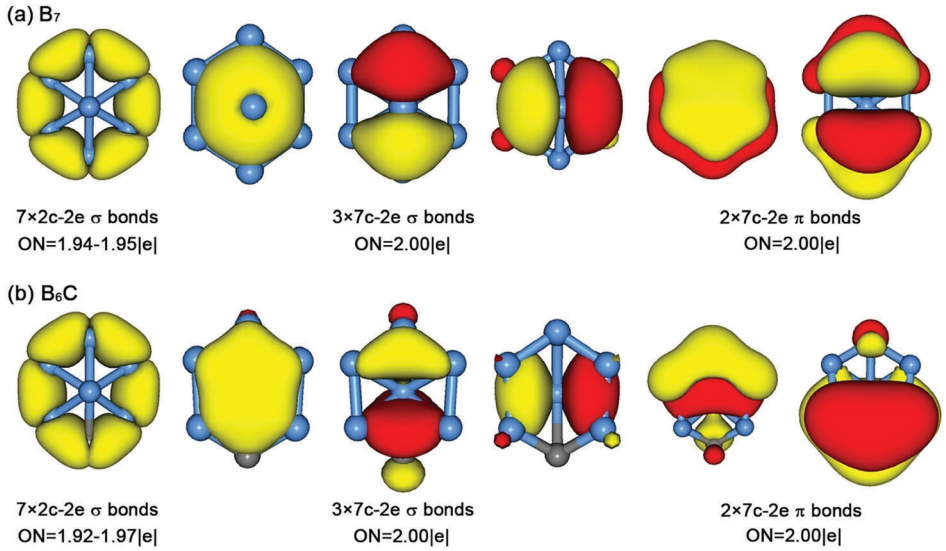

Fig. 4 AdNDP bonding patterns for wheel-like clusters: (a) B_7 and (b) B_6C. For open-shell species, one extra electron is added. Occupation numbers (ONs) are shown.

wheel-like (n = 1), elongated (n = 2, 3), or cyclic (n = 4–6), the Lewis elements are one 2c–2e B–B/B–C σ bond per peripheral link. The remaining electrons form delocalized π and σ frameworks, endowing the species (π and σ) with aromaticity, antiaromaticity, and conflicting aromaticity according to specific π and σ electron countings. The overall bonding pictures can be obtained *via* tedious, detailed CMO analyses (Fig. S8–S10, ESI†; also see the CMOs of the linear C_7 cluster in Fig. S11, ESI†) and are also borne out by AdNDP analyses. The final AdNDP schemes are illustrated in Fig. 4(b), 5, and 6, which are relatively straightforward for comprehension. Three technical notes are made here. Firstly, for an open-shell species, one extra electron is added in AdNDP analyses. Second, for circular B_3C_4, B_2C_5, and BC_6 clusters (Fig. 2(b)), both Clar and Kekule schemes are possible for delocalized π and σ bonding. We therefore chose to present in Fig. 6 our favorite Kekule scheme for B_3C_4 and Clar schemes for B_2C_5 and BC_6;[68] see their complementary Clar or Kekule schemes in Fig. S12 (ESI†). Third, certain bonds associated with delocalized π/σ frameworks have relatively low occupation numbers (ONs) below 1.7 $|e|$ in the Kekule scheme (Fig. 5 and 6; Fig. S12, ESI†), which is actually a reflection of the fact that such π/σ frameworks are more delocalized than what the Kekule scheme shows.[68]

As shown in Fig. 4(b), 5 and 6, the number of delocalized electrons in C_nB_{7-n} (n = 1–6) are 10, 9, 10, 11, 12, and 13, respectively. The electrons are split between σ and π frameworks, and the σ framework has 6, 5, 6, 6, 6, and 7 electrons, respectively. Accordingly, the π framework has 4, 4, 4, 5, 6, and 6 electrons. These numbers are tabulated in Table 1. Based on π and σ electron countings, one may intuitively conclude that: (1) the wheel-like B_6C cluster, for example, has conflicting aromaticity (4π antiaromaticity plus 6σ aromaticity). This is consistent with the elongated C_s structure (Fig. 1(b)), a characteristic structural consequence of π antiaromaticity. (2) The elongated monocyclic structures of B_5C_2 and B_4C_3 (Fig. 2(a)) are due to 4π antiaromaticity. (3) Monocyclic B_3C_4, B_2C_5, and BC_6 clusters assume a circular shape because both their π and σ frameworks are close to the "magic" sextet counting, which is one argument why we prefer the Clar schemes in AdNDP analyses for the B_2C_5 and BC_6 species (Fig. 6). In particular, B_2C_5 has exact 6π and 6σ electron countings, endowing it with (π and σ) double aromaticity.

We have so far found a solid connection between delocalized π/σ electron countings and the conformations in the C_nB_{7-n} (n = 0–6) clusters, demonstrating that wheel-like, elongated, and circular structures are entirely governed by the delocalized π/σ frameworks. Tuning the number of delocalized electrons along the series changes the π/σ electron countings and endows the species with aromaticity, antiaromaticity, or conflicting aromaticity. In particular, π antiaromaticity appears to dictate the elongated structures of B_5C_2 and B_4C_3 clusters, whereas (π and σ) double aromaticity is the major driving force for the monocyclic, circular structures of B_3C_4, B_2C_5, and BC_6. Lastly, for the linear C_7 cluster, the nature of bonding is illustrated in Fig. 7. The linear chain is linked evenly *via* 2c–2e C–C σ bonds, further superimposed by two sets of 3c–2e C–C–C π bonds (six π bonds in total). In addition, each terminal C atom has a C 2s lone-pair.

NICS values can serve as an independent, semi-quantitative measure of aromaticity in the systems, as shown in Table 1. Here, $NICS_{zz}(0)$, calculated at the ring center, primarily measures σ aromaticity/antiaromaticity; whereas $NICS_{zz}(1)$, calculated at 1 Å above the ring center, reflects π aromaticity. It is stressed that $NICS_{zz}(0)$ and $NICS_{zz}(1)$ values presented in the table, as quantitative as they appear, should be considered to be qualitative as a criterion for aromaticity, because they only qualitatively separate the contribution of σ and π *via* changing the distance between the probing point and the ring center. In principle, it is possible to dissect NICSs into NICS(σ) and NICS(π) and to perform a σ–π separation analysis, which can probe even in a quantitative sense the contribution of aromaticity related to σ and π, as suggested

Published on 16 August 2017. Downloaded by Shanxi University on 10/31/2018 8:37:25 AM.

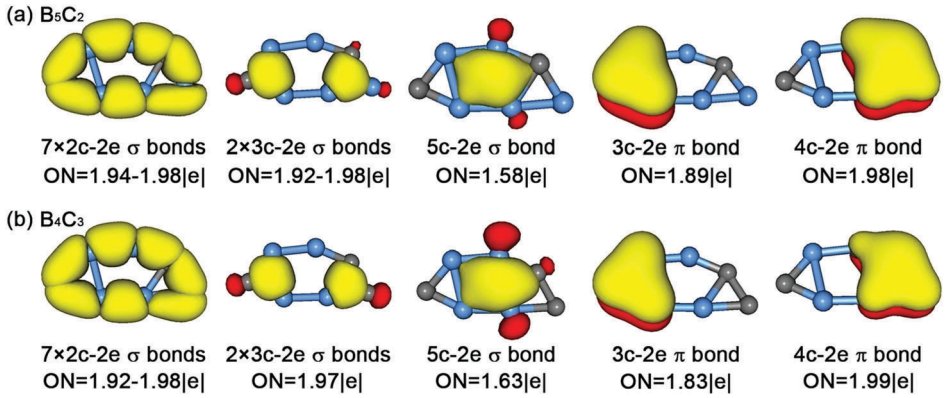

Fig. 5 AdNDP bonding patterns for elongated clusters: (a) B_5C_2 and (b) B_4C_3. For open-shell species, one extra electron is added. Occupation numbers (ONs) are shown.

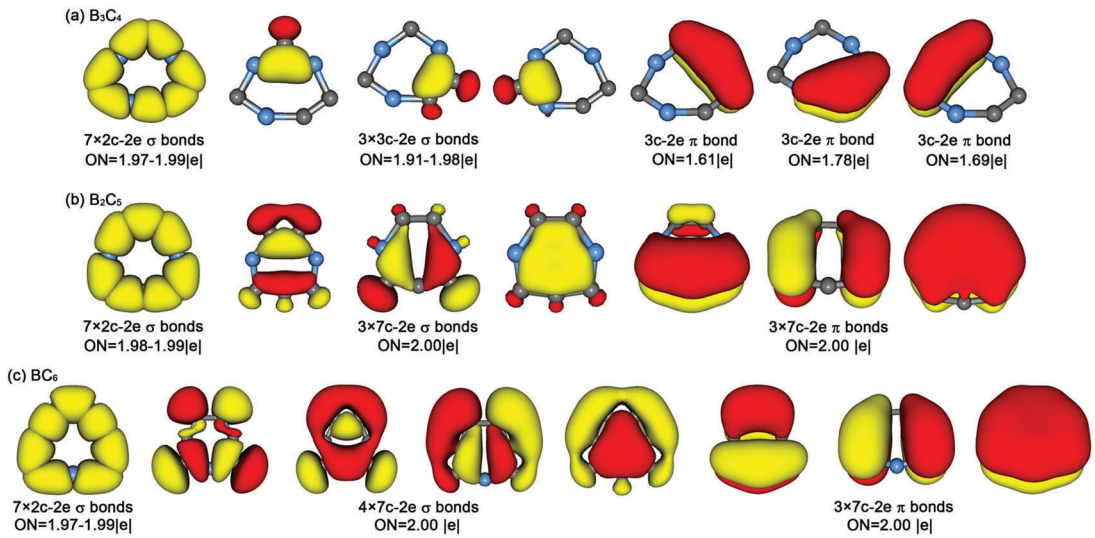

Fig. 6 AdNDP bonding patterns for monocyclic clusters: (a) B_3C_4, (b) B_2C_5, and (c) BC_6. For open-shell species, one extra electron is added. Occupation numbers (ONs) are shown.

Table 1 Calculated nucleus-independent chemical shifts in ppm for C_nB_{7-n} (n = 0–7) clusters at the ring center and at 1 Å above the center, denoted as $NICS_{zz}(0)$ and $NICS_{zz}(1)$, respectively. The number of delocalized σ and π electrons in these species are also presented

Species	B_7	B_6C	B_5C_2	B_4C_3	B_3C_4	B_2C_5	BC_6
$NICS_{zz}(0)$	−9.93	−1.60	−20.15	−24.04	−15.07	−40.40	−30.57
$NICS_{zz}(1)^a$	6.13	7.83	−1.77	−5.13	−16.51	−31.65	−28.23
σ	6	6	5	6	6	6	7
π	3	4	4	4	5	6	6

[a] For a nonplanar cluster, $NICS_{zz}(1)$ is calculated above the ring center at the concave side.

by Datta.[69] However, we believe that the current NICS data are sufficient for our purpose. First, aromaticity and antiaromaticity in the C_nB_{7-n} (n = 0–6) clusters are established herein primarily on the basis of chemical bonding analyses (that is, CMOs, AdNDP, and electron counting). Thus, NICSs only serve as an additional support and are a relatively minor issue in the study. Second, the focus of this work is the trend of evolution along the whole series and it is perfectly OK to be qualitative only. Overall, our NICS data are consistent with the CMO and AdNDP results. For example, the $NICS_{zz}(1)$ values for B_7, B_6C, B_5C_2, and B_4C_3 are either positive or close to zero, which are in line with π anti-aromaticity. There appears to be a boost in $NICS_{zz}(1)$ for B_3C_4, B_2C_5, BC_6, due to 6π aromaticity. Most remarkably, B_2C_5 has the greatest values for both $NICS_{zz}(0)$ and $NICS_{zz}(1)$ in the whole series, because it is the only species that satisfies the $(4n + 2)$ electron counting for both π and σ frameworks; that is, π and σ double aromaticity.

4.4. Why C avoids hypercoordination in the B_6C cluster?

Hypercoordination in a planar fashion, of C, B, and other main group elements, are of persistent interest in physical chemistry and theoretical chemistry since the 1970s.[70] Of equal importance is the recent discovery that C avoids hypercoordination in B–C mixed clusters.[36,71–73] A vague interpretation[73] is that C in hypercoordination contributes to delocalized bonding only, whereas C in the periphery participates in both 2c–2e bonding

 This journal is © the Owner Societies 2017

Published on 16 August 2017. Downloaded by Shanxi University on 10/31/2018 8:37:25 AM.

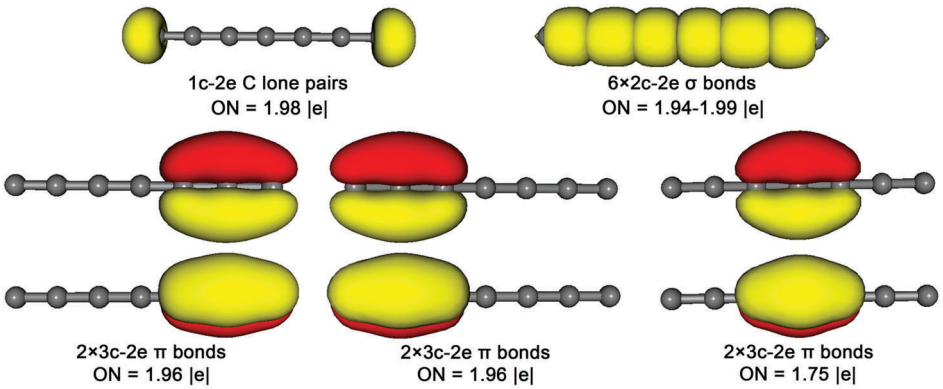

Fig. 7 AdNDP bonding pattern for the linear C_7 cluster. Occupation numbers (ONs) are shown.

and delocalized bonding. We believe that this interpretation is insufficient, because the total number of 2c–2e bonds and delocalized π and σ bonds are the same, independent of the position of the C atom (central *versus* peripheral).

The present data on the B_6C cluster allow us to address this issue. To proceed with the discussion, it is convenient to disentangle the global π/σ bonding and the peripheral Lewis elements (2c–2e σ bonds and lone-pairs) in the system: GM **a1** (C_s, $^1A'$) *versus* high energy isomer **a16** (C_{2v}, $^1A_1$) (Fig. S1, ESI†). There are both pro and con sides for structure **a1**, in which the C atom is situated in the periphery. The global π/σ frameworks for **a1** and **a16** involve a similar set of 5 delocalized CMOs, including three σ CMOs (HOMO−1, HOMO−2, and HOMO−4 for structure **a1**) and two π CMOs (HOMO and HOMO−5). The fact that C is in the periphery in **a1** is a penalty for electron delocalization: HOMO−1, HOMO−4, and HOMO−5 in **a1** are elevated in energy by as much as 0.75, 0.58, and 0.63 eV, respectively, as compared to their corresponding CMOs in **a16**. HOMO−2 is also marginally elevated by 0.06 eV. The only CMO that benefits in **a1** is the HOMO, which is stabilized by 0.77 eV relative to that in **a16**. Collectively, these 5 delocalized CMOs are destabilized by 1.25 eV (28.8 kcal mol^{-1}), which is actually a con for **a1**.

On the other hand, for the Lewis elements, structure **a1** has four peripheral 2c–2e B–B σ bonds plus two 2c–2e B–C σ bonds, which are to be compared to six peripheral 2c–2e B–B σ bonds in **a16**. Although the total number of such peripheral σ bonds is the same for **a1** and **a16**, the former gains an edge because it has two B–C σ bonds in exchange of two B–B σ bonds in **a16**. Fortunately, a B–C single bond has a dissociation energy of 393 kJ mol^{-1}, which is markedly greater than a B–B single bond (290 kJ mol^{-1}). In fact, a B–C single bond is even stronger than a C–C single bond (346 kJ mol^{-1}). This unique strength of a B–C single bond is a pro for structure **a1**, gaining an enhanced stability of ∼200 kJ mol^{-1}, or 2.07 eV, for the Lewis elements (two B–C σ bonds), which effectively compensates for the penalty in delocalized π/σ frameworks. Note that **a1** also benefits for its B1B2 and B5B4 σ bonds, which are shorter (by 0.04 Å) than those in **a16**. In terms of electrostatics, the 10 delocalized electrons in **a1** have a distribution of 3 from the center *versus* 7 from the ring, compared to 5 *versus* 5 in **a16**; the former distribution has a clear advantage in managing electrostatic interactions, which is also a pro for **a1**. These pros govern the stability of **a1** over **a16**, ultimately making it 34.62 kcal mol^{-1} lower in energy at the B3LYP level. Similar arguments should explain why C avoids hypercoordination in other B–C binary clusters.[36,71–73]

5. Conclusions

In conclusion, we have performed a quantum chemical study on the structures and chemical bonding of an extensive series of boron–carbon mixed clusters C_nB_{7-n} (n = 0–7) at the B3LYP/6-311+G(d) and single-point CCSD(T) levels, making use of an array of computational tools: Coalescence Kick global-minimum searches, natural bond orbital (NBO) atomic charges, canonical molecular orbital (CMO) analyses, adaptive natural density partitioning (AdNDP), and nucleus-independent chemical shifts (NICSs). A rich variety of structural conformations are revealed: wheel-like B_7 and B_6C, elongated B_5C_2 and B_4C_3, monocyclic B_3C_4, B_2C_5, and BC_6, and linear C_7. Successive structural transitions along the series are governed by delocalized π and σ bonding, whose number of electrons is explicitly tuned by one at a time. In particular, 4π antiaromaticity leads to the wheel-like to elongated transition, whereas 6π aromaticity drives the elongated to circular transition. The B_2C_5 cluster with 6π and 6σ electrons conforms exactly to the ($4n$ + 2) Hückel rule for both π and σ frameworks, endowing it with (π and σ) double aromaticity. The present results also shed light on the issue why C in the B_6C cluster prefers to occupy a peripheral site rather than the center and why C avoids hypercoordination. We believe that the same arguments can be extended to other B–C clusters in prior reports, such as B_6C^{2-}, B_7C^-, and B_8C.

Conflicts of interest

There are no conflicts to declare.

Acknowledgements

This work was supported by the National Natural Science Foundation of China (21573138). H. J. Z. also gratefully

Published on 16 August 2017. Downloaded by Shanxi University on 10/31/2018 8:37:25 AM.

acknowledges support from the Sanjin Scholar Distinguished Professors Program.

References

1 H. J. Zhai, L. S. Wang, A. N. Alexandrova and A. I. Boldyrev, *J. Chem. Phys.*, 2002, **117**, 7917.
2 H. J. Zhai, A. N. Alexandrova, K. A. Birch, A. I. Boldyrev and L. S. Wang, *Angew. Chem., Int. Ed.*, 2003, **42**, 6004.
3 H. J. Zhai, B. Kiran, J. Li and L. S. Wang, *Nat. Mater.*, 2003, **2**, 827.
4 A. N. Alexandrova, A. I. Boldyrev, H. J. Zhai and L. S. Wang, *J. Phys. Chem. A*, 2004, **108**, 3509.
5 I. Boustani, *Phys. Rev. B: Condens. Matter Mater. Phys.*, 1997, **55**, 16426.
6 E. Oger, N. R. M. Crawford, R. Kelting, P. Weis, M. M. Kappes and R. Ahlrichs, *Angew. Chem., Int. Ed.*, 2007, **46**, 8503.
7 F. L. Gu, X. Yang, A. C. Tang, H. J. Jiao and P. v. R. Schleyer, *J. Comput. Chem.*, 1998, **19**, 203.
8 J. E. Fowler and J. M. Ugalde, *J. Phys. Chem. A*, 2000, **104**, 397.
9 J. Aihara, H. Kanno and T. Ishida, *J. Am. Chem. Soc.*, 2005, **127**, 13324.
10 A. P. Sergeeva, D. Y. Zubarev, H. J. Zhai, A. I. Boldyrev and L. S. Wang, *J. Am. Chem. Soc.*, 2008, **130**, 7244.
11 W. Huang, A. P. Sergeeva, H. J. Zhai, B. B. Averkiev, L. S. Wang and A. I. Boldyrev, *Nat. Chem.*, 2010, **2**, 202.
12 W. L. Li, Q. Chen, W. J. Tian, H. Bai, Y. F. Zhao, H. S. Hu, J. Li, H. J. Zhai, S. D. Li and L. S. Wang, *J. Am. Chem. Soc.*, 2014, **136**, 12257.
13 Q. Chen, W. J. Tian, L. Y. Feng, H. G. Lu, Y. W. Mu, H. J. Zhai, S. D. Li and L. S. Wang, *Nanoscale*, 2017, **9**, 4550.
14 Y. J. Wang, Y. F. Zhao, W. L. Li, T. Jian, Q. Chen, X. R. You, T. Ou, X. Y. Zhao, H. J. Zhai, S. D. Li, J. Li and L. S. Wang, *J. Chem. Phys.*, 2016, **144**, 064307.
15 H. R. Li, T. Jian, W. L. Li, C. Q. Miao, Y. J. Wang, Q. Chen, X. M. Luo, K. Wang, H. J. Zhai, S. D. Li and L. S. Wang, *Phys. Chem. Chem. Phys.*, 2016, **18**, 29147.
16 H. J. Zhai, Y. F. Zhao, W. L. Li, Q. Chen, H. Bai, H. S. Hu, Z. A. Piazza, W. J. Tian, H. G. Lu, Y. B. Wu, Y. W. Mu, G. F. Wei, Z. P. Liu, J. Li, S. D. Li and L. S. Wang, *Nat. Chem.*, 2014, **6**, 727.
17 A. N. Alexandrova, A. I. Boldyrev, H. J. Zhai and L. S. Wang, *Coord. Chem. Rev.*, 2006, **250**, 2811.
18 H. J. Zhai, S. D. Li and L. S. Wang, *J. Am. Chem. Soc.*, 2007, **129**, 9254.
19 S. D. Li, H. J. Zhai and L. S. Wang, *J. Am. Chem. Soc.*, 2008, **130**, 2573.
20 H. J. Zhai, Q. Chen, H. Bai, S. D. Li and L. S. Wang, *Acc. Chem. Res.*, 2014, **47**, 2435.
21 J. O. C. Jiménez-Halla, R. Islas, T. Heine and G. Merino, *Angew. Chem., Int. Ed.*, 2010, **49**, 5668.
22 G. Martínez-Guajardo, A. P. Sergeeva, A. I. Boldyrev, T. Heine, J. M. Ugalde and G. Merino, *Chem. Commun.*, 2011, **47**, 6242.
23 Y. J. Wang, X. Y. Zhao, Q. Chen, H. J. Zhai and S. D. Li, *Nanoscale*, 2015, **7**, 16054.
24 Y. J. Wang, X. R. You, Q. Chen, L. Y. Feng, K. Wang, T. Ou, X. Y. Zhao, H. J. Zhai and S. D. Li, *Phys. Chem. Chem. Phys.*, 2016, **18**, 15774.
25 Q. Chen, W. L. Li, Y. F. Zhao, S. Y. Zhang, H. S. Hu, H. Bai, H. R. Li, W. J. Tian, H. G. Lu, H. J. Zhai, S. D. Li, J. Li and L. S. Wang, *ACS Nano*, 2015, **9**, 754.
26 A. J. Mannix, X. F. Zhou, B. Kiraly, J. D. Wood, D. Alducin, B. D. Myers, X. Liu, B. L. Fisher, U. Santiago, J. R. Guest, M. J. Yacaman, A. Ponce, A. R. Oganov, M. C. Hersam and N. P. Guisinger, *Science*, 2015, **350**, 1513.
27 B. Feng, J. Zhang, Q. Zhong, W. Li, S. Li, H. Li, P. Cheng, S. Meng, L. Chen and K. Wu, *Nat. Chem.*, 2016, **8**, 563.
28 C. R. Wang, R. B. Huang, Z. Y. Liu and L. S. Zheng, *Chem. Phys. Lett.*, 1995, **242**, 355.
29 J. D. Presilla-Márquez, P. G. Carrick and C. W. Larson, *J. Chem. Phys.*, 1999, **110**, 5702.
30 L. M. Wang, B. B. Averkiev, J. A. Ramilowski, W. Huang, L. S. Wang and A. I. Boldyrev, *J. Am. Chem. Soc.*, 2010, **132**, 14104.
31 K. Chuchev and J. J. BelBruno, *J. Phys. Chem. A*, 2004, **108**, 5226.
32 R. X. Wang, D. J. Zhang, R. X. Zhu and C. B. Liu, *THEOCHEM*, 2007, **817**, 119.
33 J. L. Shao, C. Y. He, R. W. Shi, C. Wang, X. L. Zhu and X. H. Lu, *THEOCHEM*, 2010, **961**, 17.
34 J. L. Shao, X. L. Zhu, X. H. Lu and R. W. Shi, *THEOCHEM*, 2008, **855**, 82.
35 C. Wang, W. W. Cui, J. L. Shao, X. L. Zhu and X. H. Lu, *Int. J. Quantum Chem.*, 2013, **113**, 2514.
36 Y. Pei and X. C. Zeng, *J. Am. Chem. Soc.*, 2008, **130**, 2580.
37 T. R. Galeev, A. S. Ivanov, C. Romanescu, W. L. Li, K. V. Bozhenko, L. S. Wang and A. I. Boldyrev, *Phys. Chem. Chem. Phys.*, 2011, **13**, 8805.
38 I. A. Popov, V. F. Popov, K. V. Bozhenko, I. Černušák and A. I. Boldyrev, *J. Chem. Phys.*, 2013, **139**, 114307.
39 T. F. Wang and J. H. Bowie, *Phys. Chem. Chem. Phys.*, 2009, **11**, 7553.
40 C. H. Liu, M. S. Tang and H. M. Wang, *J. Phys. Chem. A*, 2007, **111**, 704.
41 A. M. McAnoy, J. H. Bowie and S. J. Blanksby, *J. Phys. Chem. A*, 2003, **107**, 10149.
42 Z. H. Cui, M. Contreras, Y. H. Ding and G. Merino, *J. Am. Chem. Soc.*, 2011, **133**, 13228.
43 C. H. Liu, L. L. Liu, P. L. Han, M. S. Tang and H. F. Fu, *Rapid Commun. Mass Spectrom.*, 2008, **22**, 3599.
44 C. Y. He, J. L. Shao, R. W. Shi and X. L. Zhu, *Comput. Theor. Chem.*, 2011, **967**, 59.
45 J. L. Shao, R. W. Shi, C. Wang, X. L. Zhu and X. H. Lu, *J. Mol. Model.*, 2010, **16**, 939.
46 H. J. Zhai, L. S. Wang, D. Y. Zubarev and A. I. Boldyrev, *J. Phys. Chem. A*, 2006, **110**, 1689.
47 A. P. Sergeeva, B. B. Averkiev, H. J. Zhai, A. I. Boldyrev and L. S. Wang, *J. Chem. Phys.*, 2011, **134**, 224304.
48 M. Saunders, *J. Comput. Chem.*, 2004, **25**, 621.
49 P. P. Bera, K. W. Sattelmeyer, M. Saunders, H. F. Schaefer III and P. v. R. Schleyer, *J. Phys. Chem. A*, 2006, **110**, 4287.

 This journal is © the Owner Societies 2017

Published on 16 August 2017. Downloaded by Shanxi University on 10/31/2018 8:37:25 AM.

50 M. J. Frisch, G. W. Trucks, H. B. Schlegel, G. E. Scuseria, M. A. Robb, J. R. Cheeseman, G. Scalmani, V. Barone, B. Mennucci, G. A. Petersson, H. Nakatsuji, M. Caricato, X. Li, H. P. Hratchian, A. F. Izmaylov, J. Bloino, G. Zheng, J. L. Sonnenberg, M. Hada, M. Ehara, K. Toyota, R. Fukuda, J. Hasegawa, M. Ishida, T. Nakajima, Y. Honda, O. Kitao, H. Nakai, T. Vreven, J. A. Montgomery, Jr., J. E. Peralta, F. Ogliaro, M. Bearpark, J. J. Heyd, E. Brothers, K. N. Kudin, V. N. Staroverov, R. Kobayashi, J. Normand, K. Raghavachari, A. Rendell, J. C. Burant, S. S. Iyengar, J. Tomasi, M. Cossi, N. Rega, J. M. Millam, M. Klene, J. E. Knox, J. B. Cross, V. Bakken, C. Adamo, J. Jaramillo, R. Gomperts, R. E. Stratmann, O. Yazyev, A. J. Austin, R. Cammi, C. Pomelli, J. W. Ochterski, R. L. Martin, K. Morokuma, V. G. Zakrzewski, G. A. Voth, P. Salvador, J. J. Dannenberg, S. Dapprich, A. D. Daniels, Ö. Farkas, J. B. Foresman, J. V. Ortiz, J. Cioslowski and D. J. Fox, *GAUSSIAN 09, Revision D.01*, Gaussian, Inc., Wallingford, CT, 2009.
51 J. Cizek, *Adv. Chem. Phys.*, 1969, **14**, 35.
52 G. E. Scuseria and H. F. Schaefer III, *J. Chem. Phys.*, 1989, **90**, 3700.
53 G. E. Scuseria, C. L. Janssen and H. F. Schaefer III, *J. Chem. Phys.*, 1988, **89**, 7382.
54 J. A. Pople, M. Head-Gordon and K. Raghavachari, *J. Chem. Phys.*, 1987, **87**, 5968.
55 A. E. Reed, L. A. Curtiss and F. A. Weinhold, *Chem. Rev.*, 1988, **88**, 899.
56 D. Y. Zubarev and A. I. Boldyrev, *Phys. Chem. Chem. Phys.*, 2008, **10**, 5207.
57 P. V. R. Schleyer, C. Maerker, A. Dransfeld, H. J. Jiao and N. J. R. V. E. Hommes, *J. Am. Chem. Soc.*, 1996, **118**, 6317.
58 U. Varetto, *Molekel 5.4.0.8*, Swiss National Supercomputing Center, Manno, Switzerland, 2009.
59 J. VandeVondele, M. Krack, F. Mohamed, M. Parrinello, T. Chassaing and J. Hutter, *Comput. Phys. Commun.*, 2005, **167**, 103.
60 A. V. Orden and R. J. Saykally, *Chem. Rev.*, 1998, **98**, 2313.
61 C. Chowdhury and A. Datta, *J. Phys. Chem. Lett.*, 2017, **8**, 2909.
62 S. M. Pratik, C. Chowdhury, R. Bhattacharjee, S. Jahiruddin and A. Datta, *Chem. Phys.*, 2015, **460**, 101.
63 K. Bhattacharyya, A. Surendran, C. Chowdhury and A. Datta, *Phys. Chem. Chem. Phys.*, 2016, **18**, 31160.
64 A. Nijamudheen, R. Bhattacharjee, S. Choudhury and A. Datta, *J. Phys. Chem. C*, 2015, **119**, 3802.
65 J. M. García-Lastra, P. García-Fernández, F. Calle-Vallejo, A. Trueba, J. A. Aramburu and M. Moreno, *Inorg. Chem.*, 2014, **53**, 6534.
66 D. Jose and A. Datta, *Acc. Chem. Res.*, 2014, **47**, 593.
67 P. Pyykkö, *J. Phys. Chem. A*, 2015, **119**, 2326.
68 It is stressed that the Clar and Kekule schemes are basically equivalent to each other for a specific species. The Kekule scheme is a simplified, localized view of the Clar one, and in essence a B–C mixed cluster is more or less a localized system because the valence electrons and NBO atomic charges (Fig. 3) are not uniformly distributed around the ring. Nonetheless, certain clusters can indeed be more delocalized than others (B_2C_5 and BC_6 *versus* B_3C_4, for example), due to enhanced aromaticity or double aromaticity.
69 D. Jose and A. Datta, *J. Phys. Chem. C*, 2012, **116**, 24639.
70 L. M. Yang, E. Ganz, Z. F. Chen, Z. X. Wang and P. v. R. Schleyer, *Angew. Chem., Int. Ed.*, 2015, **54**, 9468.
71 B. B. Averkiev, D. Y. Zubarev, L. M. Wang, W. Huang, L. S. Wang and A. I. Boldyrev, *J. Am. Chem. Soc.*, 2008, **130**, 9248.
72 L. M. Wang, W. Huang, B. B. Averkiev, A. I. Boldyrev and L. S. Wang, *Angew. Chem., Int. Ed.*, 2007, **46**, 4550.
73 B. B. Averkiev, L. M. Wang, W. Huang, L. S. Wang and A. I. Boldyrev, *Phys. Chem. Chem. Phys.*, 2009, **11**, 9840.